JACS
JOURNAL OF THE AMERICAN CHEMICAL SOCIETY
Communication
pubs.acs.org/JACS

Deep-Ultraviolet Transparent Phosphates $RbBa_2(PO_3)_5$ and $Rb_2Ba_3(P_2O_7)_2$ Show Nonlinear Optical Activity from Condensation of $[PO_4]^{3-}$ Units

Sangen Zhao,[†] Pifu Gong,[‡,§] Siyang Luo,[‡] Lei Bai,[‡] Zheshuai Lin,*[,‡] Chengmin Ji,[†] Tianliang Chen,[†] Maochun Hong,[†,∥] and Junhua Luo*[,†,∥]

[†]Key Laboratory of Optoelectronic Materials Chemistry and Physics and [∥]State Key Laboratory of Structural Chemistry, Fujian Institute of Research on the Structure of Matter, Chinese Academy of Sciences, Fuzhou, Fujian 350002, China

[‡]Beijing Center for Crystal R&D, Key Lab of Functional Crystals and Laser Technology of Chinese Academy of Sciences, Technical Institute of Physics and Chemistry, Chinese Academy of Sciences, Beijing 100190, China

[§]University of Chinese Academy of Sciences, Beijing 100049, China

Supporting Information

ABSTRACT: It is challenging to explore deep-ultraviolet (deep-UV) nonlinear optical (NLO) materials that can achieve a subtle balance between deep-UV transparency and high NLO activity. Known deep-UV NLO materials are almost exclusively limited to borates, except few newly discovered phosphates despite their small NLO activities. Here we report two asymmetric phosphates, $RbBa_2(PO_3)_5$ (**I**) and $Rb_2Ba_3(P_2O_7)_2$ (**II**), which feature $[PO_3]_\infty$ chains and $[P_2O_7]^{4-}$ dimers formed by condensation of $[PO_4]^{3-}$ units, respectively. Remarkably, **I** achieves the desired balance, with the shortest deep-UV absorption edge at 163 nm and the largest NLO activity of 1.4 × KDP (KH_2PO_4) in deep-UV NLO phosphates. According to first-principles calculations, the enhanced macroscopic SHG response of **I** can be attributed to the $[PO_3]_\infty$ chains which exhibit significantly larger microscopic SHG coefficients as compared with the $[P_2O_7]^{4-}$ dimers.

Deep-ultraviolet (deep-UV) nonlinear optical (NLO) materials can produce coherent light of wavelengths below 200 nm, which plays a unique and crucial role in a number of scientific instruments that have opened up unprecedented opportunities to explore novel phenomena in physics and materials science.[1−6] A rigorous prerequisite for a deep-UV NLO material is that it should be transparent in the spectral region with the wavelength below 200 nm. Deep-UV NLO materials are thus almost exclusively limited to borates which possess both relatively large SHG response and short UV absorption edge.[7−9] Notable examples include a number of beryllium borates, such as $KBe_2BO_3F_2$ (KBBF),[10,11] $NaBeB_3O_6$,[12] $Na_2CsBe_6B_5O_{15}$,[13] $Na_2Be_4B_4O_{11}$, and $Li_2Na_5Be_{12}B_{12}O_{33}$,[14] and some beryllium-free borates, such as $K_3B_6O_{10}Cl$,[15] $Ba_4B_{11}O_{20}F$,[16] and $Li_4Sr(BO_3)_2$ discovered by our group.[17] It was not until quite recently that the first nonboron-containing deep-UV NLO phosphates, $Ba_3P_3O_{10}X$ (X = Cl, Br),[18] were discovered, which highlights phosphates as novel deep-UV NLO materials. Unfortunately, their SHG responses (about 0.6 × and 0.5 × KDP, KH_2PO_4) are rather small as compared to that of KBBF (~1.21 × KDP).[19]

In order to acquire enhanced SHG response, the common strategy is to introduce NLO-active structural units, such as second-order Jahn−Teller (SOJT) distorted octahedra of d^0 cation centers or stereoactive lone pair cations,[20−22] polar chalcogenide units,[23] and d^{10} cations centered polyhedra with large polar displacement.[24,25] However, the presence of large SHG response in a material is usually conflicting to short absorption edge; the aforementioned units can cause the absorption edge of a material to red-shift evidently. A notable example is the phosphate $KTiOPO_4$ (KTP);[26] the SOJT distorted TiO_6 octahedra in an aligned arrangement make the dominant contribution to the strong SHG response of KTP, but they also result in a disadvantageous absorption edge at 350 nm being far from the deep-UV region.[27] Therefore, it is always a challenge to explore applicable deep-UV NLO materials since it needs to achieve a subtle balance between deep-UV transparency and large SHG response.

It is well-known that large alkaline and alkaline-earth cations are susceptible to asymmetry and have short absorption edge. Meanwhile, the microscopic groups with tetrahedral configuration are believed to be beneficial to short UV absorption edge.[28] Since the known P-O groups are exclusively formed by asymmetric PO_4 tetrahedra, it can be expected that their synergistic combination with large cations will greatly increase the likelihood of creating new deep-UV NLO phosphates. Here, we show two asymmetric phosphates, $RbBa_2(PO_3)_5$ (**I**) and $Rb_2Ba_3(P_2O_7)_2$ (**II**), both which are deep-UV transparent and NLO-active. Remarkably, **I** achieves the desired balance, with the shortest deep-UV absorption edge at 163 nm and the largest powder SHG efficiency of 1.4 × KDP in deep-UV phosphates. First-principles calculations were carried out to elucidate the SHG origin.

Single crystals of **I** and **II** were grown through spontaneous crystallization from high-temperature melts which were prepared in platinum crucibles by melting mixtures of analytically pure Rb_2CO_3, $BaCO_3$, and $(NH_4)_2HPO_4$ at molar ratios of 1:4:10 and 2:2:5, respectively. The phase purity was confirmed by powder X-

Received: April 30, 2014
Published: June 6, 2014

   dx.doi.org/10.1021/ja504319x | J. Am. Chem. Soc. 2014, 136, 8560−8563

ray diffraction (XRD). The experimental XRD patterns well match the calculated ones based on single-crystal XRD analysis (see Figures S1 and S2). The inductively coupled plasma element analysis of **I** and **II** gave molar ratios of Rb:Ba:P = 1.1:2:5.2 and Rb:Ba:P = 2.1:3:4.1, respectively, which are consistent with the compositions determined by single-crystal XRD analysis.

I and **II** crystallize in asymmetric space groups of monoclinic *Pc* and orthorhombic $P2_12_12_1$, respectively, and their crystal structures are displayed in Figure 1. In the structure of **I**, there are

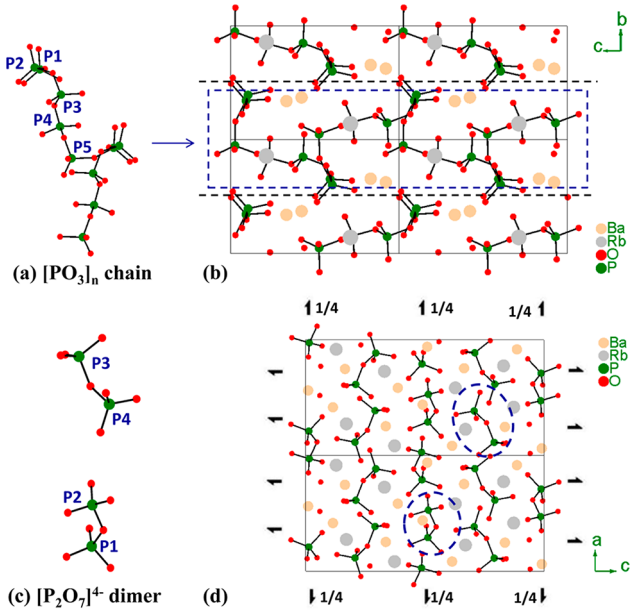

Figure 1. (a) $[PO_3]_\infty$ chain. (b) Crystal structure of **I**. (c) Two sets of $[P_2O_7]^{4-}$ dimers. (d) Crystal structure of **II**. The positions of selected 2_1 screw axes and glide planes are indicated.

five crystallographically independent phosphor atoms, which are all coordinated with four oxygen atoms to form $[PO_4]^{3-}$ tetrahedral units and further construct infinite one-dimensional (1D) $[PO_3]_\infty$ chains via corner-sharing (Figure 1a). The 1D $[PO_3]_\infty$ chains extend themselves wavily up and down the *ac* plane and are related to each other by the *c*-glide plane $(x, 1/2, z)$ (Figure 1b). In the crystal structure of **II**, there are four crystallographically independent phosphor atoms, which are all coordinated with four oxygen atoms to construct two sets of zero-dimensional (0D) $[P_2O_7]^{4-}$ dimers that are formed by two $[PO_4]^{3-}$ tetrahedral units via corner-sharing (Figure 1c). The 0D $[P_2O_7]^{4-}$ dimers are isolated from each other and operate themselves by the 2_1-screw axes, e.g., $(1/4, 0, z)$ and $(x, 1/4, 0)$ (Figure 1d). The PO_4 tetrahedra in **I** and **II** are distorted with O-P-O angles in the ranges of 99.0(3)°−120.7(3)° and 100.1(5)°−115.3(6)°, respectively, and P-O bonds in the ranges of 1.470(5)−1.634(6) Å and 1.500(11)−1.64(1) Å, respectively. Such distortions result in the asymmetric local coordination without any mirror plane symmetry in 1D $[PO_3]_\infty$ chains and 0D $[P_2O_7]^{4-}$ dimers, just like the cases of 0D $[P_3O_{10}]^{5-}$ trimers in $Ba_3P_3O_{10}X$ (X = Cl, Br).[18] In the structure of **I**, Ba atoms are 8-coordinated by O atoms with Ba-O bond lengths ranging from 2.635(6) Å to 3.059(5) Å, and Rb atoms are 10-coordinated by O atoms with Rb-O bond lengths ranging from 2.779(6) Å to 3.494(6) Å (Figure S3). In comparison, Ba atoms in **II** are 7- or 8-coordinated with Ba-O bond lengths of 2.57(1)−3.003(10) Å, and Rb atoms are 10- or 11-coordinated with Rb-O bond lengths of 2.785(10)−3.573(10) Å (Figure S4). These large Ba and Rb atoms form asymmetric polyhedra, and a further combination with the asymmetric P-O clusters results in the crystallographical asymmetry of both compounds.

The thermal stability of **I** and **II** was investigated by the differential scanning calorimetric (DSC) analysis on a NETZSCH DTA404PC thermal analyzer (the DSC was calibrated with Al_2O_3). As shown in Figure 2a, the DSC data

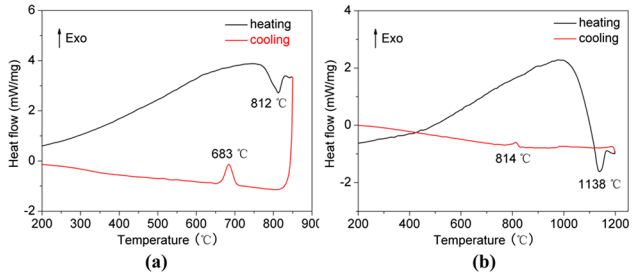

Figure 2. DSC curves of (a) **I** and (b) **II**.

of **I** show only one sharp endothermic peak around 812 °C in the heating curve and one sharp exothermic peak at 683 °C in the cooling curve, which indicates that **I** is a congruently melting compound. In this work, single crystals of **I** were obtained from its stoichiometric melt, further demonstrating that **I** melts congruently. As shown in Figure 2b, the DSC data of **II** show one sharp endothermic peak around 1138 °C in the heating curve and a very small exothermic peak at a much lower temperature of 814 °C in the cooling curve. The residues after the DSC analysis were characterized by powder XRD analysis. Their XRD pattern is distinct from that before melting (Figure S5), demonstrating that **II** melts incongruently.

UV/vis/NIR diffuse reflectance spectra were collected for both **I** and **II** on a PerkinElmer Lamda-900 UV/vis/NIR spectrophotometer. As shown in Figure 3a,b, there is no obvious absorption peak in the energy range of 6.2−1.3 eV (corresponding to a wavelength range of about 200−900 nm), indicating that both **I** and **II** are transparent down to the deep-UV spectral

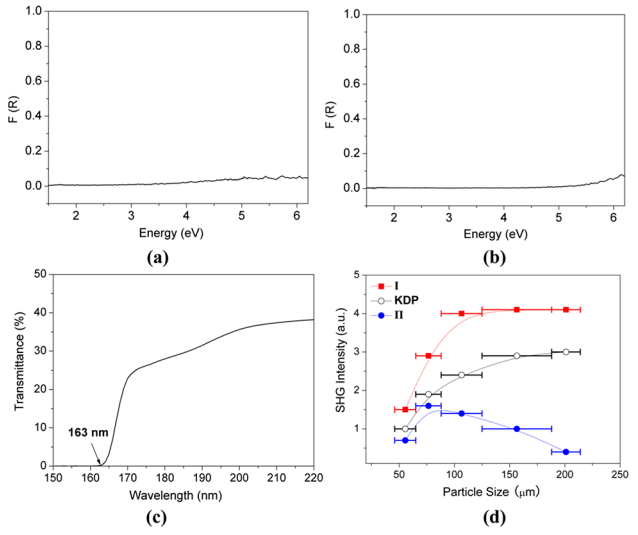

Figure 3. UV/vis/NIR diffuse reflectance spectra of (a) **I** and (b) **II**. (c) Deep-UV transmittance spectrum of **I**. (c) SHG intensity vs particle size at 1064 nm. The solid curves are drawn to guide the eyes and are not fits to the data.

dx.doi.org/10.1021/ja504319x | J. Am. Chem. Soc. 2014, 136, 8560−8563

region. To further determine the exact absorption edge, we measured the deep-UV transmittance spectrum of **I** using a spectrophotometer (VUVas2000, McPherson) in the wavelength range of 120−220 nm. A crystal with dimensions of about 4 × 4 × 1 mm^3 (Figure S6) was used for the measurement without polishing. As shown in Figure 3c, the UV absorption edge of **I** is as short as 163 nm (corresponding to a very large band gap of 7.61 eV). Such an absorption edge is shorter than that of $Ba_3P_3O_{10}Cl$ (180 nm).[18] It is also comparable to those of beryllium borates, such as KBBF (155 nm),[11] $Na_2Be_4B_4O_{11}$ (169 nm), and $LiNa_5Be_{12}B_{12}O_{33}$ (171 nm),[14] and those of beryllium-free borates, such as $Li_4Sr(BO_3)_2$ (186 nm)[17] and $K_3B_6O_{10}Cl$ (182 nm).[15] Since both **I** and **II** are asymmetric, we carried out powder SHG measurements by the Kurtz−Perry method[29] with a Q-switched Nd:YAG laser of λ = 1064 nm. Polycrystalline KDP samples were used as the references. The curves of SHG signal as a function of particle size are shown in Figure 3d. The SHG intensity of **I** increases with increasing particle size before it becomes constant, while the SHG intensity of **II** initially increases and then decreases with increasing particle size. According to the rule proposed by Kurtz and Perry,[29] **I** is phase-matchable whereas **II** is not at the wavelength of 1064 nm. In the same particle size of 125−188 μm, the SHG efficiencies of **I** and **II** are about 1.4 and 0.3 times that of KDP, respectively. The SHG efficiency of **I** is significantly larger than those of $Ba_3P_3O_{10}Cl$ (0.6 × KDP) and $Ba_3P_3O_{10}Br$ (0.5 × KDP).[18] It is also comparable to those of beryllium borates, such as KBBF (1.21 × KDP),[19] $NaBeB_3O_6$ (1.60 × KDP),[12] $Na_2CsBe_6B_5O_{15}$ (1.17 × KDP),[13] $Na_2Be_4B_4O_{11}$ (1.3 × KDP), and $LiNa_5Be_{12}B_{12}O_{33}$ (1.4 × KDP)[13] as well as that of beryllium-free $Li_4Sr(BO_3)_2$ (2.0 × KDP).[17] Therefore, **I** has promising prospects to be a good deep-UV NLO material due to its congruently melting property, short absorption edge, and large SHG response as well as the phase-matchability.

In order to elucidate the mechanism of optical properties of **I** and **II**, the first-principles calculations were performed by the plane-wave pseudopotential method implemented in the CASTEP package.[30,31] The electronic band structures of both crystals were obtained (see Figures S7 and S8). Figure 4 displays

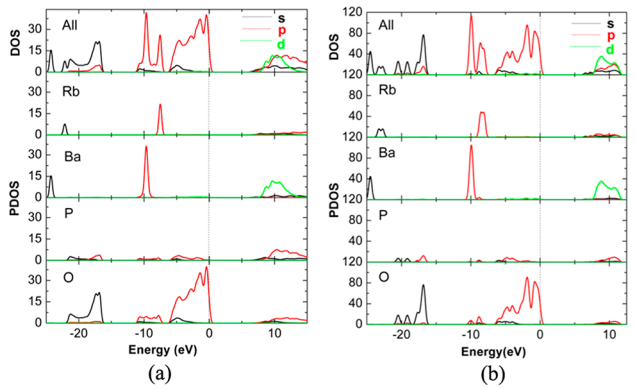

Figure 4. DOS and PDOS plots of (a) **I** and (b) **II**.

the density of states (DOS) and the partial density of states (PDOS) projected on the constitutional atoms. Several electronic characteristics can be deduced: (i) The region lower than −7 eV is composed of the isolated inner-shell states with Rb 3s3p, Ba 4s4p, P 2s2p, and O 2s orbitals, which have little interaction with neighboring atoms. (ii) The upper part of valence band (VB) is mainly composed of the p orbitals of oxygen (2p) and phosphorus (3p), indicating that there are relatively strong covalent bonds between O and P. (iii) The bottom of the conduct band (CB) consists of the mixture of the orbitals on all constituent atoms. Since the optical response of a crystal mainly originates from the electronic transitions between the VB and CB states close to the bandgap,[32] the P-O groups determine the optical properties, e.g., SHG effect; i.e., the NLO activities of **I** and **II** originate from the condensation of $[PO_4]^{3-}$ tetrahedral units that built the 1D $[PO_3]_\infty$ chains and 0D $[P_2O_7]^{4-}$ dimers, respectively. In addition, the shortened UV absorption edge of **I** (163 nm, 7.61 eV) in comparison with that of $Ba_3P_3O_{10}Cl$ (180 nm, 6.87 eV) can be explained by the presence of Cl 3p orbitals on the top of VB in the latter (see Figure S4a in ref 18), which pushes the electronic level at the VB maximum upward and thus narrows the energy bandgap. The SHG coefficient d_{ij} was calculated by the formula developed by Lin et al.[33,34] Under the restriction of Kleinman's symmetry,[35] **I** has six nonzero independent SHG coefficients owing to its *Pc* space group, while **II** has only one nonzero independent SHG coefficient because of its $P2_12_12_1$ space group. The largest two SHG coefficients for **I** are d_{12} = 0.371 pm/V and d_{13} = −0.591 pm/V, respectively (all SHG coefficients see Table 1). These

Table 1. Calculated SHG Coefficients and the Atom-Cutting Results of I and II

species	d_{ij}	total (pm/V)	Rb^+ (pm/V)	Ba^{2+} (pm/V)	P-O groups (pm/V)
I	d_{11}	0.066	0.026	−0.025	0.074
	d_{12}	0.371	−0.013	0.023	0.329
	d_{13}	−0.591	−0.013	−0.055	−0.421
	d_{15}	0.007	0.017	−0.035	0.023
	d_{24}	0.197	0.007	0.000	0.179
	d_{33}	0.073	−0.013	−0.019	0.135
II	d_{14}	0.073	0.016	−0.030	0.121

values are in good agreement with our measured value, which is 1.4 times that of KDP (d_{36}(KDP) = 0.38 pm/V).[36] In the case of **II**, the calculated, sole SHG coefficient is d_{14} = 0.073 pm/V, which is consistent with its weak powder SHG response (0.3 × KDP). Moreover, we adopted a real-space atom-cutting technique to investigate the microscopic structural origins for the SHG effects in both crystals, and the results are also given in Table 1. Evidently, the P-O groups, i.e., 1D $[PO_3]_\infty$ chains of **I** and 0D $[P_2O_7]^{4-}$ dimers of **II**, make the dominant contributions to the SHG coefficients of both compounds, whereas the contributions of the cations (Rb^+ and Ba^{2+}) are negligibly small.

The optical properties can also be elucidated from the structural features in **I** and **II**. In accordance with the anionic group theory,[37] for both compounds the P-O groups are the dominating active units, which determine the SHG coefficients. Table 2 shows the optical properties and structural characteristics of the known deep-UV NLO phosphates. It can be seen that **I** has

Table 2. Optical Properties and Structural Characteristics of Deep-UV NLO Phosphates

species	space group	P-O groups	absorption edge (nm)	SHG[a]
II[b]	$P2_12_12_1$	$[P_2O_7]^{4-}$	<200	0.3
$Ba_3P_3O_{10}Br$[c]	$P2_12_12_1$	$[P_3O_{10}]^{5-}$	<200	0.5
$Ba_3P_3O_{10}Cl$[c]	$Pca2_1$	$[P_3O_{10}]^{5-}$	180	0.6
I[b]	*Pc*	$[PO_3]_\infty$	163	1.4

[a]In multiples of KDP. [b]This work. [c]Data from ref 12.

dx.doi.org/10.1021/ja504319x | J. Am. Chem. Soc. 2014, 136, 8560−8563

almost the *shortest* absorption edge yet exhibits the *largest* SHG response in deep-UV NLO phosphates. We also note that the SHG responses follow the condensation degree trend of $[P_2O_7]^{4-}$ < $[P_3O_{10}]^{5-}$ < $[PO_3]_\infty$. This suggests that, with the prolongation of the P-O groups from 0D $[P_2O_7]^{4-}$ dimers and 0D $[P_3O_{10}]^{5-}$ trimers to infinite 1D $[PO_3]_\infty$ chains, the NLO-active groups become more vulnerable to be perturbed by an intense electric field of a laser, so produce a more pronounced SHG response,[38] as confirmed by the atom-cutting analysis. In fact, the observation, microscopic units condensed into 1D chains are beneficial to the generation of large SHG effect, has also been demonstrated in infrared NLO materials, e.g., $A_3Ta_2AsS_{11}$ (A = K and Rb)[23] and $AAsSe_2$ (A = Li, Na).[39] Therefore, we believe that it is an effective approach to designing deep-UV transparent phosphates with high NLO-activity via the condensation of $[PO_4]^{3-}$ units, specifically, into 1D chains. Further in-depth investigations are progressing.

In summary, two asymmetric phosphates, $RbBa_2(PO_3)_5$ (**I**) and $Rb_2Ba_3(P_2O_7)_2$ (**II**), were synthesized. Remarkably, **I** achieves a desirable balance, with the shortest UV absorption edge at 163 nm and the largest SHG response of 1.4 × KDP in deep-UV NLO phosphates. Theory calculations reveal that the enhanced macroscopic SHG response of **I** is attributed to the 1D $[PO_3]_\infty$ chains which exhibit significantly larger microscopic SHG coefficients as compared with the 0D $[P_2O_7]^{4-}$ dimers. This work provides a new approach to designing highly NLO-active phosphates while maintaining deep-UV transparency via the condensation of $[PO_4]^{3-}$ units into 1D chains. Future efforts will be devoted to the growth of large crystals and related physical property studies for compound **I** as well as the in-depth investigations on the SHG mechanism.

■ ASSOCIATED CONTENT

Supporting Information

Crystallographical and additional data. This material is available free of charge via the Internet at http://pubs.acs.org.

■ AUTHOR INFORMATION

Corresponding Author

jhluo@fjirsm.ac.cn; zslin@mail.ipc.ac.cn

Notes

The authors declare no competing financial interest.

■ ACKNOWLEDGMENTS

This work was financially supported by the National Natural Science Foundation of China (21222102, 21373220, 51102231, 21171166, 11174297, 91022036), the National Basic Research Project of China (2010CB630701, 2010CB933501, 2011CB922204, 2011CB935904). S.Z. thanks Profs. Yicheng Wu and Guochun Zhang at TIPC for their guidance during his graduate school.

■ REFERENCES

(1) Meng, J. Q.; Liu, G. D.; Zhang, W. T.; Zhao, L.; Liu, H. Y.; Jia, X. W.; Mu, D. X.; Liu, S. Y.; Dong, X. L.; Zhang, J.; Lu, W.; Wang, G. L.; Zhou, Y.; Zhu, Y.; Wang, X. Y.; Xu, Z. Y.; Chen, C. T.; Zhou, X. J. *Nature* **2009**, *462*, 335.

(2) Gao, L. B.; Ren, W. C.; Xu, H. L.; Jin, L.; Wang, Z. X.; Ma, T.; Ma, L. P.; Zhang, Z. Y.; Fu, Q.; Peng, L. M.; Bao, X. H.; Cheng, H. M. *Nat. Commun.* **2012**, *3*, 699.

(3) Reshak, A. H.; Chen, X.; Auluck, S.; Kityk, I. *J. Chem. Phys.* **2008**, *129*, 204111.

(4) Reshak, A. H.; Auluck, S.; Kityk, I. *Appl. Phys. A: Mater. Sci. Process.* **2008**, *91*, 451.

(5) Reshak, A. H.; Chen, X.; Kityk, I.; Auluck, S. *Curr. Opin. Solid State Mater. Sci.* **2007**, *11*, 33.

(6) Reshak, A. H.; Auluck, S.; Kityk, I. *J. Solid State Chem.* **2008**, *181*, 789.

(7) Becker, P. *Adv. Mater.* **1998**, *10*, 979.

(8) Reshak, A. H.; Auluck, S.; Kityk, I. *J. Phys.: Condens. Matter* **2008**, *20*, 145209.

(9) Reshak, A. H.; Auluck, S.; Majchrowski, A.; Kityk, I. *PMC Phys. B* **2008**, *1*, 8.

(10) Cyranoski, D. *Nature* **2009**, *457*, 953.

(11) Xia, Y. N.; Chen, C. T.; Tang, D. Y.; Wu, B. C. *Adv. Mater.* **1995**, *7*, 79.

(12) Wang, S. C.; Ye, N.; Li, W.; Zhao, D. *J. Am. Chem. Soc.* **2010**, *132*, 8779.

(13) Wang, S. C.; Ye, N. *J. Am. Chem. Soc.* **2011**, *133*, 11458.

(14) Huang, H. W.; Liu, L. J.; Jin, S. F.; Yao, W. J.; Zhang, Y. H.; Chen, C. T. *J. Am. Chem. Soc.* **2013**, *135*, 18319.

(15) Wu, H.; Pan, S.; Poeppelmeier, K. R.; Li, H.; Jia, D.; Chen, Z.; Fan, X.; Yang, Y.; Rondinelli, J. M.; Luo, H. *J. Am. Chem. Soc.* **2011**, *133*, 7786.

(16) Wu, H. P.; Yu, H. W.; Yang, Z. H.; Hou, X. L.; Su, X.; Pan, S. L.; Poeppelmeier, K. R.; Rondinelli, J. M. *J. Am. Chem. Soc.* **2013**, *135*, 4215.

(17) Zhao, S. G.; Gong, P. F.; Bai, L.; Xu, X.; Zhang, S. Q.; Sun, Z. H.; Lin, Z. S.; Hong, M. C.; Chen, C. T.; Luo, J. H. *Nat. Commun.* **2014**, *5*, 4019.

(18) Yu, P.; Wu, L. M.; Zhou, L. J.; Chen, L. *J. Am. Chem. Soc.* **2014**, *136*, 480.

(19) Chen, C. T.; Wang, G. L.; Wang, X. Y.; Xu, Z. Y. *Appl. Phys. B: Laser Opt.* **2009**, *97*, 9.

(20) Halasyamani, P. S.; Poeppelmeier, K. R. *Chem. Mater.* **1998**, *10*, 2753.

(21) Zhao, S. G.; Jiang, X. X.; He, R.; Zhang, S. Q.; Sun, Z. H.; Luo, J. H.; Lin, Z. S.; Hong, M. C. *J. Mater. Chem. C* **2013**, *1*, 2906.

(22) Phanon, D.; Gautier-Luneau, I. *Angew. Chem., Int. Ed. Engl.* **2007**, *46*, 8488.

(23) Bera, T. K.; Jang, J. I.; Ketterson, J. B.; Kanatzidis, M. G. *J. Am. Chem. Soc.* **2009**, *131*, 75.

(24) Zhao, S. G.; Zhang, J.; Zhang, S. Q.; Sun, Z. H.; Lin, Z. S.; Wu, Y. C.; Hong, M. C.; Luo, J. H. *Inorg. Chem.* **2014**, *53*, 2521.

(25) Yu, H.; Wu, H.; Pan, S.; Yang, Z.; Hou, X.; Su, X.; Jing, Q.; Poeppelmeier, K. R.; Rondinelli, J. M. *J. Am. Chem. Soc.* **2014**, *136*, 1264.

(26) Reshak, A. H.; Kityk, I.; Auluck, S. *J. Phys. Chem. B* **2010**, *114*, 16705.

(27) Driscoll, T. A.; Hoffman, H. J.; Stone, R. E.; Perkins, P. E. *J. Opt. Soc. Am. B* **1986**, *3*, 683.

(28) Chen, C. T.; Sasaki, T.; Li, R. K.; Wu, Y. C.; Lin, Z. S.; Mori, Y.; Hu, Z. G.; Wang, J. Y.; Uda, S.; Yoshimura, M.; Kaneda, Y. *Nonlinear Optical Borate Crystals: Principles and Applications*; Wiley-VCH Press: Weinheim, 2012.

(29) Kurtz, S. K.; Perry, T. T. *J. Appl. Phys.* **1968**, *39*, 3798.

(30) Payne, M. C.; Teter, M. P.; Allan, D. C.; Arias, T. A.; Joannopoulos, J. D. *Rev. Mod. Phys.* **1992**, *64*, 1045.

(31) Clark, S. J.; Segall, M. D.; Pickard, C. J.; Hasnip, P. J.; Probert, M. J.; Refson, K.; Payne, M. C. *Z. Kristallogr.* **2005**, *220*, 567.

(32) Lee, M. H.; Yang, C. H.; Jan, J. H. *Phys. Rev. B* **2004**, *70*, 235110.

(33) Lin, J.; Lee, M. H.; Liu, Z. P.; Chen, C. T.; Pickard, C. J. *Phys. Rev. B* **1999**, *60*, 13380.

(34) Lin, Z. S.; Lin, J.; Wang, Z. Z.; Wu, Y. C.; Ye, N.; Chen, C. T.; Li, R. K. *J. Phys.: Condens. Matter* **2001**, *13*, R369.

(35) Kleinman, D. A. *Phys. Rev.* **1962**, *126*, 1977.

(36) Eckardt, R. C.; Masuda, H.; Fan, Y. X.; Byer, R. L. *IEEE J. Quantum Electron.* **1990**, *26*, 922.

(37) Chen, C. *Sci. Sin.* **1979**, *22*, 756.

(38) Jiang, X. X.; Zhao, S. G.; Lin, Z. S.; Luo, J. H.; Bristowe, P. D.; Guan, X. G.; Chen, C. T. *J. Mater. Chem. C* **2014**, *2*, 530.

(39) Bera, T. K.; Jang, J. I.; Song, J. H.; Malliakas, C. D.; Freeman, A. J.; Ketterson, J. B.; Kanatzidis, M. G. *J. Am. Chem. Soc.* **2010**, *132*, 3484.